Stabilization of Alfvén Eigenmodes in DIII-D via Controlled Energetic Ion Density Ramp and Validation of Theory and Simulations

S. X. Tang, T. A. Carter, and N. A. Crocker
University of California, Los Angeles, Los Angeles, California 90095, USA

W. W. Heidbrink and J. B. Lestz
University of California, Irvine, Irvine, California 92697, USA

R. I. Pinsker, K. E. Thome, and M. A. Van Zeeland
General Atomics, San Diego, California 92121, USA

E. V. Belova
Princeton Plasma Physics Laboratory, Princeton, New Jersey 08540, USA

(Received 17 November 2020; accepted 19 March 2021; published 16 April 2021)

Fast-ion driven Alfvén waves with frequency close to the ion cyclotron frequency ($f = 0.58 f_{ci}$) excited by energetic ions from a neutral beam are stabilized via a controlled energetic ion density ramp for the first time in a fusion research plasma. The scaling of wave amplitude with injection rate is consistent with theory for single mode collisional saturation near marginal stability. The wave is identified as a shear-polarized global Alfvén eigenmode excited by Doppler-shifted cyclotron resonance with fast ions with sub-Alfvénic energetic ions, a first in fusion research plasmas.

DOI: 10.1103/PhysRevLett.126.155001

The interplay of Alfvén waves, energetic particles, and wave damping is an important process in magnetized plasmas in space, laboratory, and astrophysical settings. High energy cosmic rays can resonantly excite Alfvén waves, which in turn can scatter these rays and lead to transport [1]. In the Earth's radiation belts, energetic protons can excite electromagnetic ion cyclotron waves that contribute to scattering and precipitation of trapped relativistic electrons [2]. In magnetically confined plasmas for fusion energy research, such as tokamaks, energetic particles are present due to heating schemes [e.g., neutral beam injection (NBI)] and fusion reactions. These processes can excite a variety of Alfvén waves confined to the plasma, Alfvén eigenmodes, that can enhance scattering and loss of energetic ions [3] by creating gradients in the ion velocity distribution at the resonance. Across all of these settings, wave-particle interaction and damping are at the heart of the wave excitation and particle scattering processes.

Compressional (CAEs) and global (GAEs) Alfvén eigenmodes driven through resonance with cyclotron motion of energetic particles (Doppler-shifted cyclotron resonance or DCR) have been found to correlate with enhanced core electron transport in the National Spherical Torus Experiment (NSTX) [4]. Understanding the role of these waves in electron thermal transport is essential for developing a predictive capability for current and future fusion experiments. In particular, future burning plasmas will be dominantly heated by energetic alpha particles from fusion reactions which can excite AEs and consequently drive anomalous transport.

This Letter reports the first observation of an energetic ion density stability threshold for the excitation of AEs in a fusion research plasma in the DIII-D tokamak, which is consistent with theoretical expectations of the instability being determined by the competition between resonant fast-ion drive and damping processes. The relationship between mode power and injection rate is consistent with theoretical scaling for collisional saturation near marginal stability [5]. These waves, with frequencies close to the ion cyclotron frequency ($f \sim 0.58 f_{ci}$), are identified as shear-polarized GAEs excited by DCR with energetic ions from NBI—the first observation of GAEs excited by sub-Alfvénic fast ions. GAEs have been observed in the same frequency range as CAEs in the spherical tokamaks START [6], MAST [7], and NSTX [8] under super-Alfvénic conditions. While previous studies in DIII-D and ASDEX Upgrade of energetic-particle-driven instabilities in this frequency range ($f \sim 0.6 f_{ci}$) called them CAEs [9,10], the measurements presented here demonstrate that these instabilities can also be GAEs excited by DCR with sub-Alfvénic ions. Understanding these modes and how their properties respond to changes in the fast-ion distribution could provide a spectroscopic technique for diagnosing energetic ions in tokamak plasmas.

The experiment on DIII-D was performed on beam-heated plasmas with injection of up to 3 MW of a < 75 keV

deuterium neutral beam, which was sub-Alfvénic under the experimental parameters. DIII-D operated at toroidal field $B_t = 1.28$–2.0 T and plasma current I_p was varied to keep B_t/I_p (which controls field geometry) constant, with electron and ion temperatures of ∼1.2 keV and ∼1 keV, and electron density $n_e \sim 3.45 \times 10^{13}$ cm^{-3} on axis. Fast magnetic fluctuations ($f = 1$–100 MHz) were measured with a pair of toroidally oriented (i.e., nearly parallel to the field) magnetic field sensing loops [11].

Mode instability is expected to be directly related to gradients in the distribution of ions sourced by the exciting NBI beam. DIII-D features a neutral beam (known as 150RT [12]) at the 150° toroidal position with tangency radius $R_{\mathrm{TAN}} \approx 74$ cm that injects in the plasma current direction, counter to the toroidal field, which was tilted downward [12,13] by 16.4°, allowing for off-axis heating and current drive. This resulted in more perpendicular injection and exploration of a wider parameter space.

DIII-D beams can independently vary the energy and injection rate of neutral particles [14] within certain limits while maintaining acceptable beam divergence. For a given density and magnetic field, controlling the beam energy allows the resonance to be selected, while controlling the injection rate allows gradients in the distribution to be controlled and thus potentially determining the stability threshold.

In this experiment, the beam injection rate was ramped down by ∼40% during discharges. These scans were performed at magnetic fields ranging from $B_t \sim 1.2$–2.0 T and beam energies from $V_b \sim 60$–80 keV. Many of the injection rate ramps were performed with no observed thresholds. High frequency AEs were observed at most $B_t \leq 1.8$ T, but the only observed mode threshold occurred during an injection rate scan of the 150RT beam at constant energy of $V_b \sim 75$ keV for a $B_t = 1.28$ T discharge. This threshold was repeatable, as approximately the same threshold value was observed during several repeat discharges with the same plasma parameters and injection rate scans.

The excitation of a highly coherent spectrum of modes was observed after the 150RT beam began injecting. Figure 1(a) shows the cross-spectrum of the magnetic fluctuation level ($|\delta b|^2$) versus frequency and time on a logarithmic color scale, masked to show only portions of the spectrum within 60 dB, or 6 orders of magnitude, of the maximum mode power. Mode onset was at $t = 2260$ ms, and the modes were observed at frequencies of $f \sim 5500$–5600 kHz, or $f \sim 0.58 f_{ci}$, where the cyclotron frequency was $f_{ci} = 9460$ kHz at the magnetic axis, $R = 1.72$ m, and the Alfvén velocity was $v_A = 3.26 \times 10^6$ m/s on axis for this plasma.

The spectrum at $t = 2260$ ms consists of a broader band, lower power structure at $f \sim 5550$ kHz, combined with two narrow band modes, one with high power at $f \approx 5520$ kHz and one with lower power at $f \approx 5490$ kHz. The $f \approx 5520$ kHz narrow band peak is overwhelmingly higher

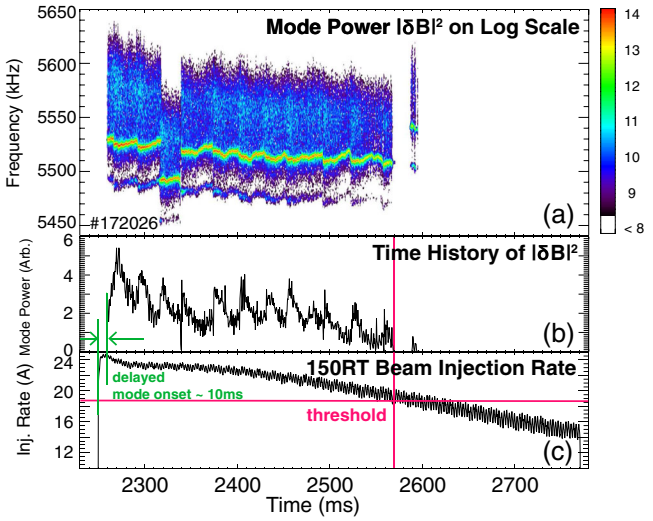

FIG. 1. (a) $|\delta b|^2$ spectrum on a logarithmic scale showing a highly coherent spectrum of high-frequency Alfvén eigenmodes at $f \sim 5550$ kHz, under a 60 dB power mask. Mode power $|\delta b|^2$ vs time (b) and beam injection rate vs time (c). Mode onset is ∼10 ms after turn-on of the 150RT beam, and the mode shuts off once beam injection rate crosses a threshold of ∼18.5 A.

power than the other peaks by > 3 orders of magnitude. The noise level of the diagnostic was > 6 orders of magnitude below this peak.

The mode power $|\delta b|^2$ becomes vanishingly small as the beam injection rate drops below a threshold of ∼18.5 A. (For convenience, the injection rate is calculated as beam power divided by energy in keV and is expressed in amps. Each beam neutral sources deuterium ions with half, third, and full energy.) The mode onset is 10 ms after beam turn-on, as expected due to a delay needed to build up resonant fast ions for mode drive. This delay is also likely caused in part by a remnant population of fast ions from a beam with different injection geometry that turned off ∼20 ms before the 150RT beam turn-on, as discussed below. The slowing-down time of the beam ions is $t < 50$ ms, calculated from the transport modeling code TRANSP [15,16].

Figures 1(b) and 1(c) show the time history of mode power with relation to the injection rate of the exciting beam. Once the injection rate crosses a certain threshold at $t \sim 2575$ ms, the mode amplitude abruptly drops 60 dB in power in < 1 ms. No delay is expected between crossing the threshold and stabilization because the beam distribution is evolving very slowly. B_t and I_p were constant during this time range, and other parameters such as temperature and density were effectively constant with variations of $< 12\%$. The modes were briefly reexcited shortly after at $t \sim 2585$ ms, with a higher frequency mode becoming the dominant mode in the spectrum, but shutting off immediately. This reexcitation is likely due to a concurrent sawtooth event causing small changes to the equilibrium and altering the fast-ion distribution. A double sawtooth crash is also responsible for the brief change in the

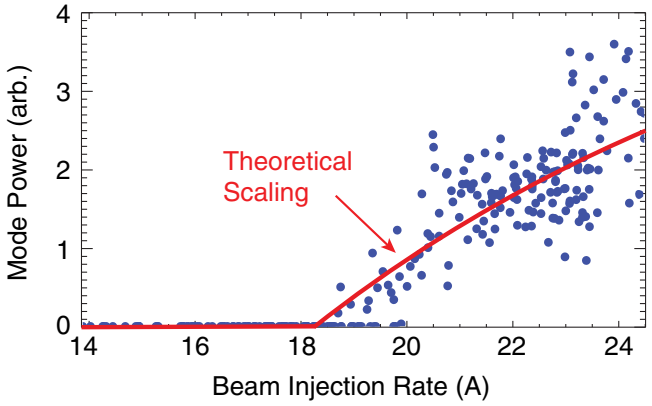

FIG. 2. Mode power $|\delta b|^2$ versus beam injection rate I_b shows that the mode is unstable for a threshold of $I_b \sim 18.5$ A. The theoretical scaling $|\delta b|^2 \sim (1 - I_{b,\mathrm{threshold}}/I_b)$ is shown in red.

spectrum at $t \sim 2320$ ms, where the lower frequency mode at $f \sim 5490$ kHz temporarily becomes the dominant, higher power mode.

Figure 2 shows mode power $|\delta b|^2$ versus beam injection rate I_b with a threshold for excitation at ~18.5 A. Because sawteeth were occurring in the plasma throughout the lifetime of the mode, only the points within the 7 ms preceding a sawtooth crash are considered for determining the scaling of mode power and injection rate. This window is chosen because it allows for maximum relaxation to the distribution without sawteeth, and the minimum time between sawtooth crashes is 14 ms.

The observed threshold is consistent with a fundamental property of resonant AEs: growth rate is set by competition between fast-ion drive and damping processes (e.g., Landau damping). This property was demonstrated in simulations of CAEs where an instability threshold was observed by varying the beam density without changing the shape of the distribution [17]. The study argued that fast-ion drive increases with beam density such that there is some critical value where drive from fast ions balances damping from other sources, leading to a beam density threshold. This argument given for CAEs in simulation is also valid for other energetic ion driven AEs. A similar beam density threshold is expected in this experiment, as designed, because the slow injection rate ramp is expected to approximately produce a distribution that changes self-similarly over time (i.e., changing only by a scale factor).

The mode power scaling as seen in Fig. 2 is consistent with predictions for single mode collisional saturation near marginal stability [5], $|\delta b|^2 \sim (1 - \gamma_d/\gamma_L) \sim (1 - I_{b,\mathrm{threshold}}/I_b)$, where γ_d is the growth rate from fast-ion drive and γ_L is the damping rate, with correlation coefficient $R^2 = 0.54$. A conclusive quantitative comparison is precluded by regular sawtooth oscillations which modulate the mode power by 50%. The observed beam injection rate threshold implies $\gamma_d/\gamma_L > 0.84$, indicating that the mode was near marginal stability during the entire beam ramp. Previous simulations of CAEs found a much stronger saturation scaling of $|\delta b|^2 \sim \gamma^4 \sim (I_b - I_{b,\mathrm{threshold}})^4$ due to being in the collisionless regime and often far from marginal stability [17].

In practice, this simple picture of a self-similar distribution evolution is complicated for a short period after beam turn-on by transients in the fast-ion population, as well as a remnant population of low energy fast ions that existed before beam turn-on, which affected the shape of the distribution. The threshold observed at the end of the ramp is unlikely to be affected by this early period; however, sawteeth, which cause intermittent fast-ion transport, are a more significant complication because the mode is at marginal stability. It should be noted that since the mode is near marginal stability, the strong modulation of mode amplitude by sawteeth at earlier times may result from only minor changes in the distribution function or bulk plasma.

The fast-ion population was analyzed to determine the resonant particles and the source of mode drive. The ORB_GC code [18] was used to calculate the characteristic poloidal and toroidal orbit frequencies (ω_ϕ and ω_θ) using a constants of motion approach. Fast-ion drive of AEs comes from resonant ions satisfying the orbit-averaged resonance equation [19]:

$$\omega - n\omega_\phi + p\omega_\theta - \ell\langle\omega_{ci}\rangle = 0, \tag{1}$$

where n is the toroidal mode number; ω_ϕ and ω_θ are positive for passing ions moving in the beam direction; and $\langle\omega_{ci}\rangle$ is the orbit-averaged cyclotron frequency. $p = m + s$ where m is the poloidal mode number and s is the toroidicity-induced sideband number (or resonance order), and s, ℓ are integers, with $\ell = 0$ corresponding to direct resonance and $\ell = 1$ corresponding to Doppler-shifted cyclotron resonance. For this analysis, ORB_GC was modified to include a gyrophase integration along one poloidal orbit, outputting an orbit-averaged cyclotron frequency $\langle\omega_{ci}\rangle$.

The transport modeling code TRANSP was used to model the evolution of the fast-ion distribution as a function of pitch, energy, position, and time. TRANSP is a time-dependent equilibrium and transport solver for tokamak plasma discharges [20]. The NUBEAM [21] module, a Monte Carlo package for evaluating the deposition, slowing down, and thermalization of fast ions in tokamaks, was used in TRANSP to predict the fast-ion distribution everywhere in (R, z) space. In this analysis, NUBEAM used the full reconnection Kadomtsev model [22] for sawtooth oscillations, and assumed no anomalous fast-ion diffusion otherwise. TRANSP and ORB_GC resonance analysis were managed via the OMFIT [23] modeling framework.

TRANSP shows a population of high energy particles appearing after beam turn-on that can drive the mode. Figure 3 shows the fast-ion population, versus pitch and energy, immediately after mode onset at $t = 2261$ ms.

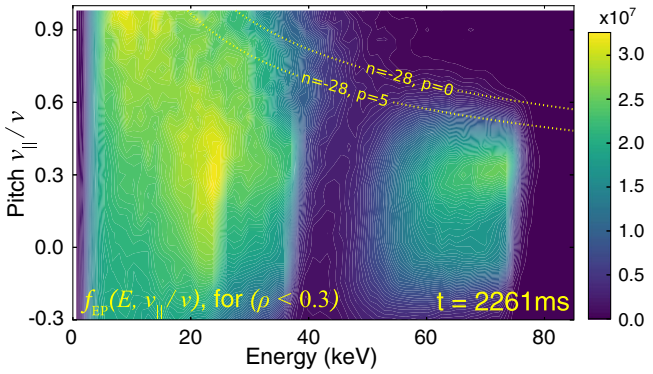

FIG. 3. Fast-ion density as a function of pitch and energy, averaged over $\rho < 0.3$, after mode onset at $t = 2261$ ms. Resonance lines for $p = 0$, 5, $n = -28$ are plotted.

The distribution shown is averaged over $\rho < 0.3$, the region over which the q profile is flat, where ρ is the normalized effective radius based on toroidal flux, and q is given approximately by rB_t/RB_p. Before beam turn-on, the population consists of a lower energy, slowing-down remnant created by a beam with different injection geometry that switched off ~20 ms prior. By the time the mode becomes unstable, approximately 10 ms after beam turn-on, a peak at high energy (> 60 keV) with pitch $v_\parallel/v \gtrsim 0.3$ has emerged (Fig. 3).

In general, the CAE-GAE drive from fast ions γ_{EP} is an integral over velocity space gradients of the fast-ion distribution. Since anisotropy is large, one term typically dominates [24]:

$$\gamma_{\mathrm{EP}} \propto -n_{\mathrm{EP}} \int h(\chi, v) \frac{\partial f_{\mathrm{EP}}(\chi, v)}{\partial \chi} d\chi \Big|_{v_\parallel = v_{\parallel,\mathrm{res}}}. \quad (2)$$

Here, $\chi = v_\parallel/v$ is the fast-ion pitch, and $h(\chi, v)$ is a positive function including finite Larmor radius effects and other terms which weight velocity space (the full definition is in Eq. (21) of Ref. [24]). The integral is taken along the $v_\parallel = v_{\parallel,\mathrm{res}}$ resonance contour shown in Fig. 3. Equation (2) is valid for subcyclotron modes driven by the $\ell = 1$ DCR —those driven instead by $\ell = 0$ or $\ell = -1$ would have opposite leading sign (in addition to differing h functions). f_{EP} is the normalized fast-ion distribution $[\int f_{\mathrm{EP}}(\boldsymbol{v}) d^3\boldsymbol{v} = 1]$ and the partial derivative $\partial f_{\mathrm{EP}}/\partial\chi$ is taken at constant energy. The value of n_{EP} determines the fast-ion number density.

After mode onset, Fig. 3 shows that the resonance lines for a range of p values intersect a region at pitch of ~0.6 and energy of 60–75 keV where $\partial f_{\mathrm{EP}}/\partial\chi < 0$, leading to fast-ion drive. Here, $p = 0$ corresponds to $s = 0$ for the observed frequency through the finite-frequency corrected dispersion relations [24].

Analysis of the fast-ion population in Fig. 3 shows the mode is likely a GAE from considerations of the dispersion relations and the DCR resonance equation $\omega_{ci} \approx \omega - k_\parallel v_\parallel$, which is an approximation of Eq. (1) with $\ell = 1$. From the dispersion relations, CAEs must have parallel phase velocity of $\omega/k_\parallel > v_A$, while GAEs have $\omega/k_\parallel < v_A$. The resonant population in Fig. 3 peaks at high energy for a pitch of $v_\parallel/v \sim 0.3$ and has little to no particles above pitch of $v_\parallel/v \sim 0.7$. For the given frequency and beam energy, the only particles present are sub-Alfvénic and have $v_0/v_A \leq 0.8$, where v_0 is the injection velocity. From Eq. (1), without large sideband resonances ($s \gg 1$), the $\ell = 0$ resonance requires super-Alfvénic ($v_\parallel/v_A > 1$) particles for CAEs. The $|\ell| = 1$ resonance at this frequency corresponds to $v_\parallel/v_A = 0.9$. Since $v_0/v_A \leq 0.8$, neither of these resonances can be satisfied for CAEs without a large toroidal sideband number s. Mode resonances are implausible for large s, because small s is expected for strong wave-particle interactions [25]. This mode is highly unlikely to be a CAE.

GAEs form below the minimum of the Alfvén continuum at a minimum in the q profile and are typically core localized [26,27]. The q profile significantly impacts shear Alfvén wave propagation via $k_\parallel$, which is given by $k_\parallel \approx (n - m/q)/R$. This plasma features a peaked density profile and $q \sim 1$ for $r < 20$ cm ($\rho < 0.3$), rising steeply for $r > 20$ cm indicating a location near the magnetic axis.

From the DCR resonance equation $\omega_{ci} \approx \omega - k_\parallel v_\parallel$, for passing particles the lowest possible $\omega/k_\parallel$ occurs for $k_\perp \sim 0$, and any nonvanishing $k_\perp$ pushes the resonance lines to the higher pitch region of the population with less particles. Because $k_\perp \sim 0$ is the most plausible resonance, an $m = 0$ mode is consistent with the data to minimize $k_\perp$. Stability considerations further reinforce this conclusion, as the fast-ion drive for $\ell = 1$ GAEs is predicted to be largest for modes with $k_\parallel \gg k_\perp$ [24]. Using the dispersion relation from Ref. [24], a GAE with $m = 0$ at this frequency has toroidal mode number $|n| = 28$. An $n = +28$ mode is ruled out because satisfying the resonance equation requires an implausibly large sideband number s. For direct resonance ($\ell = 0$), even larger values of $|s|$ are needed. The $n = -28$, $p = 0$ line in Fig. 3 passes through the region of the high energy peak at a pitch where $\partial f_{\mathrm{EP}}/\partial\chi < 0$, which is required for fast-ion drive. A relatively small sideband number, up to $s \sim 8$, moves the resonance lines closer to the peak, as shown by the $p = 5$ line. A reliable mode number measurement was unable to be experimentally obtained because the path length difference between the diagnostic channels is unknown at the time of the experiment and will be the subject of future work.

These results are consistent with recent observations [28] and simulations [27] of GAE excitation and suppression in NSTX-U. Moreover, the beam density threshold can be explained by considering Eq. (2)—as the beam density is ramped down over time, $\partial f_{\mathrm{EP}}/\partial\chi$ changes minimally, so γ_{EP} decreases in time with n_{EP}. Eventually fast-ion drive

becomes smaller than damping from the thermal plasma, and the mode rapidly decays away. Quantitatively, analytic theory [24] predicts that GAEs are driven unstable by a neutral beam distribution with normalized injection velocity $v_0/v_A = 0.8$ and peak $v_\parallel/v \approx 0.3$ when $0.5 < f/f_{ci} < 0.8$. The observed mode frequency $f/f_{ci} = 0.58$ is comfortably within this range. The frequency of these modes in the plasma frame is $f = f_{\text{measured}} + nf_{\text{ROT}} \sim 0.6 f_{ci}$, where the plasma rotation is estimated to be $f_{\text{ROT}} \sim 7$ kHz [29]. Importantly, this theory takes into account finite frequency corrections to the Alfvén dispersion relations, which are necessary for quantitative accuracy for frequencies at a large fraction of f_{ci}.

This identification as a GAE is also consistent with simulations using the Hybrid MHD code HYM [17] for a DIII-D discharge (No. 172019) very similar to that for Fig. 1. HYM is a δf initial value solver that couples a thermal fluid plasma to a population of full-orbit energetic ions. The simulations, which used a resistive MHD model for the thermal plasma, looked for unstable modes within a broad range of toroidal mode numbers and found unstable counterpropagating GAEs with $f \gtrsim 0.6 f_{ci}$ for $n = -22$–-25. GAEs were the most unstable mode for all toroidal harmonics in these simulations, and a broad range of sidebands ($\Delta p \sim 10$) made significant contributions to mode drive.

The measurements presented here agree well with simulations and analytic theory around these high-frequency Alfvén waves. The controlled stabilization of these modes demonstrates that the instability, excited through Doppler-shifted cyclotron resonance with fast ions, is determined by the competition between fast-ion drive and damping processes. This is the first observation of an energetic ion density stability threshold for these waves in a fusion research plasma, which is important in understanding their role in thermal confinement in future burning plasmas. The scaling of mode power with beam injection rate agrees with analytic theory for single mode collisional saturation near marginal stability. Analysis of the fast-ion population shows that these modes are likely excited by a resonant high energy subset of the population, and this mode is identified as a global Alfvén eigenmode—the first observation of a GAE excited by sub-Alfvénic beam ions.

J. B. Lestz acknowledges V. N. Duarte for helpful discussions. This material is based upon work supported by the U.S. Department of Energy, Office of Science, Office of Fusion Energy Sciences, using the DIII-D National Fusion Facility, a DOE Office of Science user facility, under Awards No. DE-FC02-04ER54698, No. DE-SC0020337, No. DE-AC02-09CH11466, No. DE-SC0011810, No. DE-FG02-99ER54527, and No. DE-SC0019352.

[1] E. G. Zweibel, Phys. Plasmas **24**, 055402 (2017).
[2] B. Eliasson and K. Papadopoulos, Plasma Phys. Controlled Fusion **59**, 104003 (2017).
[3] W. W. Heidbrink, Phys. Plasmas **15**, 055501 (2008).
[4] D. Stutman, L. Delgado-Aparicio, N. Gorelenkov, M. Finkenthal, E. Fredrickson, S. Kaye, E. Mazzucato, and K. Tritz, Phys. Rev. Lett. **102**, 115002 (2009).
[5] H. L. Berk, B. N. Breizman, and M. Pekker, Phys. Rev. Lett. **76**, 1256 (1996).
[6] K. G. McClements, M. P. Gryaznevich, S. E. Sharapov, R. J. Akers, L. C. Appel, G. F. Counsell, C. M. Roach, and R. Majeski, Plasma Phys. Controlled Fusion **41**, 661 (1999).
[7] L. C. Appel, T. Fülöp, M. J. Hole, H. M. Smith, S. D. Pinches, R. G. L. Vann (MAST Team), Plasma Phys. Controlled Fusion **50**, 115011 (2008).
[8] N. A. Crocker, E. D. Fredrickson, N. N. Gorelenkov, W. A. Peebles, S. Kubota, R. E. Bell, A. Diallo, B. LeBlanc, J. E. Menard, M. Podestà *et al.*, Nucl. Fusion **53**, 043017 (2013).
[9] W. W. Heidbrink, E. D. Fredrickson, N. N. Gorelenkov, T. L. Rhodes, and M. A. Van Zeeland, Nucl. Fusion **46**, 324 (2006).
[10] R. Ochoukov, R. Bilato, V. Bobkov, S. C. Chapman, R. Dendy, M. Dreval, H. Faugel, A. Kappatou, Y. O. Kazakov, M. Mantsinen *et al.*, Nucl. Fusion **60**, 126043 (2020).
[11] K. E. Thome, D. C. Pace, R. I. Pinsker, O. Meneghini, C. A. del Castillo, and Y. Zhu, Rev. Sci. Instrum. **89**, 10I102 (2018).
[12] W. W. Heidbrink, M. A. Van Zeeland, B. A. Grierson, C. M. Muscatello, J. M. Park, C. C. Petty, R. Prater, and Y. B. Zhu, Nucl. Fusion **52**, 094005 (2012).
[13] C. Murphy, M. Abrahim, P. Anderson, H. Chiu, H. Grunloh, M. Hansink, K. Holtrop, R.-M. Hong, A. Kellman, D. Kellman *et al.*, in *Proceedings of the 2011 IEEE/NPSS 24th Symposium on Fusion Engineering, Chicago* (2011), pp. 16.
[14] D. C. Pace, M. E. Austin, L. Bardoczi, C. S. Collins, B. Crowley, E. Davis, X. Du, J. Ferron, B. A. Grierson, W. W. Heidbrink *et al.*, Phys. Plasmas **25**, 056109 (2018).
[15] B. A. Grierson, X. Yuan, M. Gorelenkova, S. Kaye, N. C. Logan, O. Meneghini, S. R. Haskey, J. Buchanan, M. Fitzgerald, S. P. Smith *et al.*, Fusion Sci. Technol. **74**, 101 (2018).
[16] F. Poli, J. Sachdev, J. Breslau, M. Gorelenkova, and X. Yuan, TRANSPv18.2 [Computer Software], 2018, https://doi.org/10.11578/dc.20180627.4.

[17] E. V. Belova, N. N. Gorelenkov, N. A. Crocker, J. B. Lestz, E. D. Fredrickson, S. X. Tang, and K. Tritz, Phys. Plasmas **24**, 042505 (2017).
[18] M. A. Van Zeeland, W. W. Heidbrink, R. K. Fisher, M. García Muñoz, G. J. Kramer, D. C. Pace, R. B. White, S. Aekaeslompolo, M. E. Austin, J. E. Boom *et al.*, Phys. Plasmas **18**, 056114 (2011).
[19] N. N. Gorelenkov and C. Z. Cheng, Nucl. Fusion **35**, 1743 (1995).
[20] R. J. Goldston, D. C. McCune, H. H. Towner, S. L. Davis, R. J. Hawryluk, and G. L. Schmidt, J. Comput. Phys. **43**, 61 (1981).
[21] A. Pankin, D. McCune, R. Andre, G. Bateman, and A. Kritz, Comput. Phys. Commun. **159**, 157 (2004).
[22] B. B. Kadomtsev, Sov. J. Plasma Phys. **1**, 4 (1975).
[23] O. Meneghini, S. P. Smith, L. L. Lao, O. Izacard, Q. Ren, J. M. Park, J. Candy, Z. Wang, C. J. Luna, V. A. Izzo *et al.*, Nucl. Fusion **55**, 083008 (2015).
[24] J. B. Lestz, N. N. Gorelenkov, E. V. Belova, S. X. Tang, and N. A. Crocker, Phys. Plasmas **27**, 022513 (2020).
[25] R. Nazikian, N. N. Gorelenkov, B. Alper, H. L. Berk, D. Borba, R. V. Budny, G. Y. Fu, W. W. Heidbrink, G. J. Kramer, M. A. Makowski *et al.*, Phys. Plasmas **15**, 056107 (2008).
[26] N. N. Gorelenkov, E. Fredrickson, E. Belova, C. Z. Cheng, D. Gates, S. Kaye, and R. White, Nucl. Fusion **43**, 228 (2003).
[27] E. V. Belova, E. D. Fredrickson, J. B. Lestz, and N. A. Crocker, Phys. Plasmas **26**, 092507 (2019).
[28] E. D. Fredrickson, E. V. Belova, D. J. Battaglia, R. E. Bell, N. A. Crocker, D. S. Darrow, A. Diallo, S. P. Gerhardt, N. N. Gorelenkov, B. P. LeBlanc, and M. Podestà (NSTX-U Team), Phys. Rev. Lett. **118**, 265001 (2017).
[29] R. Seraydarian and K. Burrell, Rev. Sci. Instrum. **57**, 2012 (1986).